Polymer 50 (2009) 3828–3834

Contents lists available at ScienceDirect

Polymer

journal homepage: www.elsevier.com/locate/polymer

Understanding crystal nucleation in solution-segregated polymers

Liyun Zha, Wenbing Hu*

Department of Polymer Science and Engineering, State Key Laboratory of Coordination Chemistry, School of Chemistry and Chemical Engineering, Nanjing University, 210093 Nanjing, China

ARTICLE INFO

Article history:
Received 30 January 2009
Received in revised form
11 April 2009
Accepted 4 June 2009
Available online 10 June 2009

Keywords:
Solution
Phase diagram
Crystal nucleation

ABSTRACT

We report dynamic Monte Carlo simulations of crystal nucleation in polymer bulk phase segregated from solutions. We found that poorer solvent enhances crystal nucleation in the concentrated phase of polymers. In addition, when the solvent becomes poor enough, crystal nucleation prefers to occur at the diffuse interfaces. The results are consistent with the predictions from theoretical phase diagrams, but something different from immiscible polymer blends. The surface-enhanced crystallization may explain the bowl-shaped crystal aggregates observed experimentally in poor solvent.

1. Introduction

Liquid–liquid demixing and polymer crystallization are two basic phase transitions in multi-component polymer materials. Current investigations, however, often targeted one of these phase transitions and overlooked their interplay. As a matter of fact, the interplay of polymer phase transitions reveals the diversity of practical paths toward the multi-stage and hierarchical self-assembly of multi-component polymeric systems.

In polymer solutions, the first experimental measurement for phase diagrams exhibiting both liquid–liquid demixing and polymer crystallization was reported by Richards dating back to 1946 [1]. Flory made an introduction to this issue in his classic textbook [2]. In his recent book, Cheng made a summary on the experimental progress of this issue [3]. The interplay of phase transitions makes one major kind of thermoreversible sol–gel transitions in polymer solutions, as reviewed by Keller in 1995 [4]. In this case, polymer crystallization will freeze the evolution of the gel structure made by prior spinodal decomposition, so the interplay of these thermally induced processes dominates structure formation of microcellular foams as well as microporous membranes [5]. Recently, by means of dynamic Monte Carlo simulations of polymer solutions, we studied polymer crystal nucleation enhanced by prior metastable liquid–liquid demixing [6], as well as the morphologies of polymer crystallites modulated by prior spinodal decomposition [7]. Even in the extremely diluted polymer solutions like in a single homopolymer chain, the intramolecular crystal nucleation can be greatly accelerated by the prior hydrophobic-like collapse transition, which sheds light on the fast pathway of protein folding [8].

In polymer blends, the experimental measurement of phase diagrams of polyolefin blends in which only one component appears crystallizable was reported by Wang et al. in 2002 [9]. Molecular theory and simulations have demonstrated that, liquid–liquid demixing can be driven solely by the component-selective crystallizability of polymers in polymer blends [10], and the demixing will be further enhanced by thermal fluctuations toward crystalline order in the vicinity of the melting point [11].

Recently, Zhang et al. observed that crystal nucleation in immiscible polymer blends can be enhanced by the decrease of annealing time at a slightly higher temperature for prior spinodal decomposition [12]. Such an observation could be attributed to the interface-enhanced crystal nucleation. Theoretical phase diagrams and molecular simulations have verified that those polymers diluted at diffuse interfaces of immiscible polymer blends contain higher melting points and thus stronger thermodynamic driving force for crystal nucleation [13]. Similar experimental observations also exist in polyethylene solutions, where Schaaf et al. have investigated the bowl-shaped abnormal crystal aggregates grown in poor solvent and have proposed the idea of interface-enhanced crystal nucleation [14]. Such an idea has not yet been verified by the theoretical and simulation studies of polymer solutions, and thus constitutes the main issue addressed in our present report.

In this report, we performed theoretical calculations of phase diagrams and dynamic Monte Carlo simulations of crystal nucleation in solution-segregated polymers. The results will show that poorer solvent enhances polymer crystal nucleation in the

* Corresponding author. Tel.: +86 25 83596667; fax: +86 25 83317761.
E-mail address: wbhu@nju.edu.cn (W. Hu).

0032-3861/$ – see front matter © 2009 Elsevier Ltd. All rights reserved.
doi:10.1016/j.polymer.2009.06.005

concentrated bulk phase; in addition, a preference of crystal nucleation occurs at the interfaces only when the solvent becomes poor enough. These results are in accord with the predictions of theoretical phase diagrams, but be something different from immiscible polymer blends. The differences can be explained by a comparison of theoretical phase diagrams between polymer solutions and polymer blends. Our observation may provide evidence to the interpretation of the bowl-shaped abnormal crystal aggregates observed in experiments.

The content of this paper is organized as follows. After Introduction, we make theoretical calculations of phase diagrams in polymer solutions, followed with a brief description of simulation techniques and a report of simulation results. The paper ends up with a summary of our conclusions.

2. Theoretical phase diagrams

Polymer solutions have been well understood since the lattice model of polymers was successfully applied to calculate the mixing entropy, in addition to the mean-field treatment of mixing interactions (represented as B for each mixing pair of monomer and solvent) [15]. The well-known Flory–Huggins theory has become a paradigm in the study of statistical thermodynamics of multicomponent polymer systems such as polymer solutions [15], polymer blends [16], semiflexible polymer solutions [17], diblock copolymers [18], and polymer networks [19]. The mixing interactions will drive liquid–liquid demixing in polymer solutions. Recently, we employed local anisotropic interactions of polymers (represented as E_P for each pair of bonds packing parallel in the lattice model) as the molecular driving force for polymer crystallization [20]. Both phase diagrams for liquid–liquid demixing and polymer crystallization can thus be calculated by the developed mean-field lattice statistical theory [21]. This allows us to study the interplay between two kinds of phase transitions.

For homogeneous polymer solutions containing n_2 polymer chains, each having r monomers, and being mixed with n_1 solvent sites in a regular lattice (the total volume $n = rn_2 + n_1$), the partition function is thus given by [21]

$$Z = \left(\frac{n}{n_1}\right)^{n_1}\left(\frac{n}{n_2}\right)^{n_2}\left(\frac{q}{2}\right)^{n_2} e^{-(r-1)n_2} z_c^{(r-2)n_2} z_m^{rn_2} z_p^{(r-1)n_2}, \quad (1)$$

where

$$z_c \equiv 1 + (q-2)\exp\left(-\frac{E_C}{kT}\right),$$

$$z_m \equiv \exp\left[-(q-2)\cdot\frac{n_1}{n}\cdot\frac{B}{kT}\right],$$

$$z_p \equiv \exp\left\{-\frac{q-2}{2}\cdot\left[1-\frac{2(r-1)n_2}{qn}\right]\cdot\frac{E_P}{kT}\right\};$$

q is the coordination number of the lattice, E_C is the conformational energy for each collinear connection of two consecutive bonds along the backbone chain, E_P is the parallel-packing interaction for two non-bound bonds, B is the net mixing interactions for each pair of monomer and solvent; k is the Boltzmann's constant and T the temperature. The mixing free energy change is thus obtained as

$$\frac{\Delta F_{mix}}{nkT} = \phi_1 \ln \phi_1 + \frac{\phi_2}{r}\ln\phi_2 + \phi_1\phi_2\left[(q-2)\frac{B}{kT} + \left(1-\frac{2}{q}\right)\left(1-\frac{1}{r}\right)^2\frac{E_P}{kT}\right], \quad (2)$$

where ϕ_1 and ϕ_2 are the volume fractions of solvent and polymers, respectively. According to the equivalence of chemical potentials (denoted as μ) between two coexisting phases (denoted by $'$ and $''$, respectively), as given by

$$\begin{cases} \mu_1' = \mu_1'' \\ \mu_2' = \mu_2'' \end{cases}, \quad (3)$$

the liquid–liquid binodal can be calculated. When we calculate each kind of phase diagrams in the homogeneous phase, we disregard another kind of phase transitions potentially coexisting in reality. This means that we disregard all the practical instability and metastability in the present theoretical calculation.

At the liquid–solid coexistence curves, there also exists the equivalence of chemical potentials between liquid and crystalline states, as given by

$$\mu^S - \mu^0 = \mu^L - \mu^0, \quad (4)$$

where μ^0 is the chemical potential of polymers at the fully ordered ground state. Since the free energy ΔF of crystalline polymers is close to their ground state, we assume the approximation result

$$\mu^S - \mu^0 = \frac{\partial \Delta F^S}{\partial n_2} = \frac{\Delta F^S}{n_2} \approx 0. \quad (5)$$

The chemical potential of the liquid phase can be derived from the partition function shown in Eq. (1), so one can obtain the equilibrium melting point for variable solution compositions of polymers according to Eq. (4).

The results for equilibrium phase diagrams are shown in Fig. 1, with both the energy parameters and kT normalized by E_C. In practice, we preset E_P/E_C fixed at one to maintain the molecular driving force for crystallization under a good flexibility of chains, B/E_C variable to reflect the solvent quality, and kT/E_C specified for the reduced temperature. One can see that the larger the B/E_C values, the higher the liquid–liquid binodals, and hence the larger the intercepted polymer concentrations on the liquid–solid coexistence curves.

If we compared the liquid–solid phase diagrams of segregated polymer solutions with immiscible polymer blends demonstrated

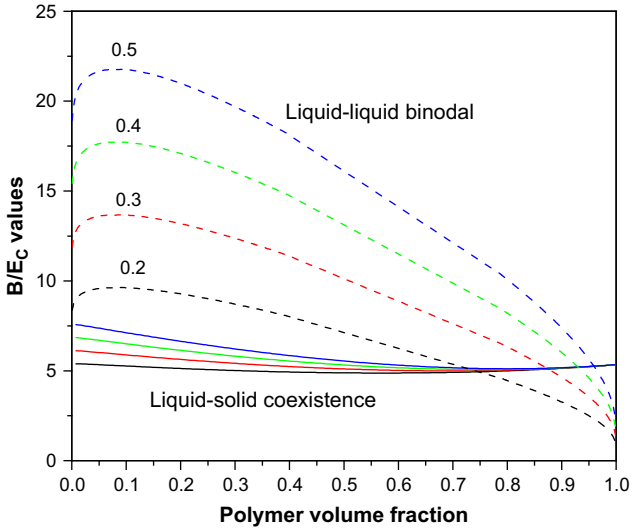

Fig. 1. Phase diagrams of polymer solutions for 128-mers with variable B/E_C values as denoted and $E_P/E_C = 1$. The curves are calculated from the developed lattice statistical theory [21]. The dashed curves are for liquid–liquid binodal, and the solid curves are for liquid–solid coexistence in the same sequence of temperatures as denoted for the dashed curves.

as the inset in Fig. 2, their differences are obvious at the concentrated end. On dilution from the concentrated end, polymer solutions exhibit a local depression of melting points before rising-up on further dilution, while polymer blends show simply rising-up of melting points. This difference can be attributed to the significant mixing entropy in the mixing free energy of polymer solutions (see Eq. (2)), while in polymer blends the mixing entropy becomes negligible with large chain lengths applied for both components.

One can see from Fig. 2 that at a fixed temperature, e.g. 4.5 E_C/k, polymer concentrations in the segregated bulk phases vary with different B/E_C values. The higher concentrations correspond to higher melting points of polymers on the liquid–solid coexistence curves. This tendency gives rise to larger supercoolings for higher concentrations at the fixed crystallization temperature, implying stronger thermodynamic driving forces for crystal nucleation. In conclusion, poorer solvent will enhance crystal nucleation in the bulk polymer phase.

Fig. 2 also shows that most parts of the liquid–solid coexistence curve are deeply buried under the liquid–liquid binodal curve. This implies that on cooling the prior demixing changes polymer concentrations and hence most of polymers stay in the bulk phase where they cannot be diluted to get those high melting points in the dilution region. However, at the diffuse interfaces of the concentrated polymer phase, some polymers will be forced to make exposure to poor solvent and hence these polymers are actually reaching the dilution region. Supposing that polymers are diluted at the interfaces presumably with the volume fraction 0.5 (diffuse interfaces actually contain a gradient of concentrations), one can find from Fig. 2 that when B/E_C becomes larger than 0.3, the melting points of polymers at the volume fraction 0.5 appear as higher than those in the bulk phase at the crystallization temperature 4.5. For $B/E_C = 0.2$ and 0.3, the melting points at the volume fraction 0.5 are still lower than those in the bulk phase segregated at $T = 4.5$ E_C/k. In other words, when the solvent quality becomes poor enough to make the melting point of interface polymers higher than bulk polymers, crystal nucleation of interface polymers can be further enhanced. This interface effect contains an enthalpic origin, the same effect as in the previously reported case of immiscible polymer blends [13].

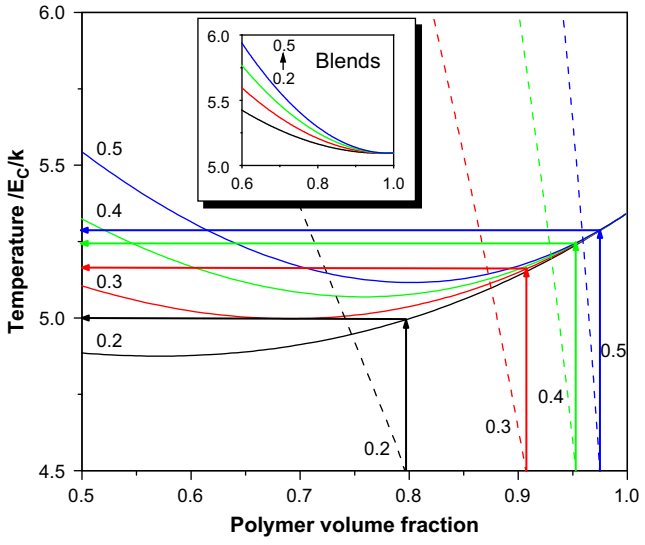

Fig. 2. Enlarged phase diagrams of polymer solutions reproduced from Fig. 1 for 128-mers with variable B/E_C values as denoted and $E_P/E_C = 1$. The dashed curves are for liquid–liquid binodal, and the solid curves are for liquid–solid coexistence curves. The arrows indicate the concentrations of the bulk polymer phases at $T = 4.5$ E_C/k and their melting points in comparison with the melting points at the interfaces (the volume fraction 0.5). The inset figure is for liquid–solid coexistence curves of polymer blends labeled with the corresponding B/E_C values [13].

3. Simulation techniques

The thermodynamic protocols used as the above theoretical phase diagrams can be realized in dynamic Monte Carlo simulations of lattice polymers in solutions, which will provide a quantitative verification to the theoretical predictions. To this end, we employed the lattice model of polymer solutions constituted by 1024 chains, each polymer chain consecutively occupying 128 lattice sites (monomers) in a 64^3 cubic lattice. So the total volume fraction of polymers is set as 0.5. The rest single vacancy sites were separated into two parts for different functions: 16,384 sites (volume fraction 0.0625) represented free volumes that were randomly distributed in the system without any thermal interactions, and the others stood for poor solvent. Polymer chains were performing micro-relaxation with periodic boundary conditions, while each step of micro-relaxation carried out the jumping of monomers into an available vacancy neighbor, with partial sliding diffusion along the chain if necessary [21]. Double occupation of monomers and the crossing of bonds were forbidden to mimic the volume exclusion of polymer chains. Small amount of free volumes were necessary for maintaining high mobility of polymers in the strongly segregated phase. The unit of time evolution, one Monte Carlo (MC) cycle, was defined as the amount of trial moves equal to the total amount of lattice sites. The initially homogeneous polymer solutions were prepared by allowing polymer chains to relax into the equilibrium random coils under athermal conditions.

The conventional Metropolis sampling algorithm was also employed with a potential energy barrier in each step of micro-relaxation, as given by

$$\frac{\Delta E}{kT} = \frac{cE_C + pE_P + bB}{kT} = \left(c + p\frac{E_P}{E_C} + b\frac{B}{E_C}\right)\frac{E_C}{kT}, \tag{6}$$

where c, p, and b were the net changes in non-collinear connection, in non-parallel packing, and in mixing pairs, respectively.

In the following, we first establish the well-oriented interfaces between two segregated phases, and then observe crystal nucleation in the concentrated polymer phase under thermodynamic conditions parallel with theoretical predictions.

4. Simulation results and discussion

We first established the equilibrium of spontaneous phase separation in the homogeneous polymer solution at the concentration 0.5. To this end, we temporarily switched off the driving force for crystallization, i.e. $E_P/E_C = 0$, and switched on the driving force for phase separation, i.e. $B/E_C = 0.1$, at a low temperature 1.5 E_C/k. It is well known that in polymer solutions the early stage of phase separation often generates randomly oriented and well distributed interfaces, either by spinodal decomposition or by nucleation, and the post-stage Ostwald ripening is dominated by the long-distance diffusion that is extremely slow for polymers. In order to accelerate phase separation and to specify the locations of interfaces, we artificially introduced a temporarily higher probability along a pair of directions from $Z = 1$ toward 32 and from $Z = 64$ toward 33 respectively (2% higher than other directions) for each monomer to choose a vacancy neighbor. Such a kinetic bias will not break the detailed balance of Monte Carlo sampling. Polymers therefore prefer to accumulate in the central area along Z-axis. When phase separation approaches at equilibrium after 2.7×10^5 MC cycles, two interfaces between segregated phases

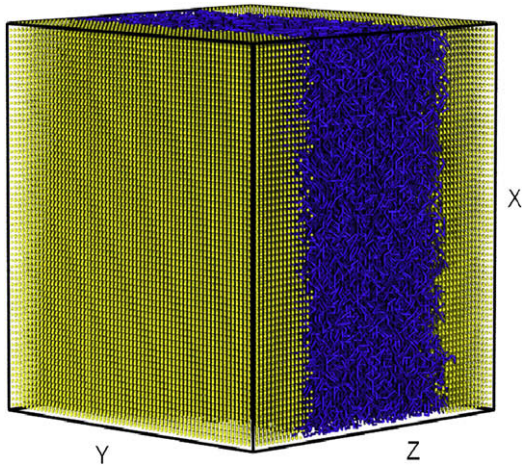

Fig. 3. Snapshot of the phase-separated polymer solutions for 128-mers with the volume fraction 0.5 under the conditions of $E_P/E_C = 0$, $B/E_C = 0.1$ and $T = 1.5\ E_C/k$ in the 64^3 lattice box. Polymer bonds are drawn in dark/blue tiny cylinders, and the vacancy sites are drawn in bright/yellow tiny spheres. (For interpretation of the references to colour in this figure legend, the reader is referred to the web version of this article.)

have been well established, as demonstrated by the snapshot shown in Fig. 3. The distribution of monomers along the direction normal to the interfaces, i.e. the *Z*-axis, is shown in Fig. 4. One can see that the interfaces are rather flat and sharp.

Next, we switched on the driving force for crystal nucleation, i.e. $E_P/E_C = 1$, under variable higher B/E_C values with no more artificial forces to orient polymer diffusion, and put the prepared sample at a chosen high temperature ($T = 4.5\ E_C/k$) to observe the largest crystallites generated by thermal fluctuations. Before making any statistics, we annealed the segregated sample for 2×10^4 MC cycles under each set of solvent quality to remove the memory of sample preparation. Such a time period of isothermal annealing should be sufficient to adapt the sample system for a new B/E_C value without any significant change in phase construction. The distributions of monomers along the direction normal to the flat interfaces with variable B/E_C values are summarized in Fig. 5. One can see that the poorer the solvent quality (the larger B/E_C values), the higher the

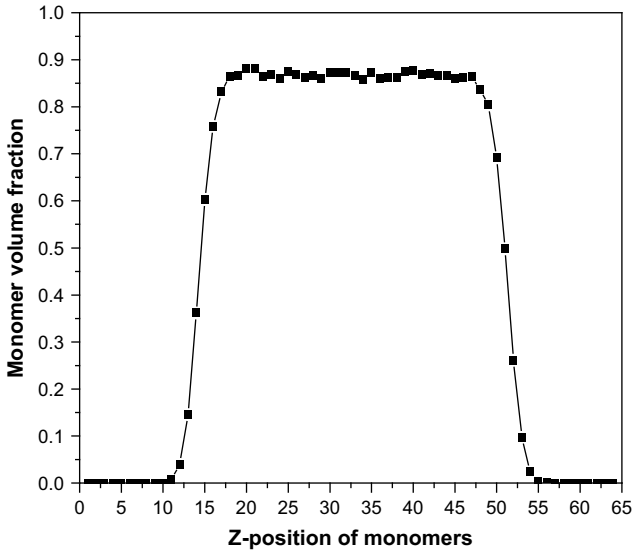

Fig. 4. Monomer distributions along the direction normal to the flat interfaces, i.e. along the *Z*-axis, for the sample prepared in Fig. 1. The monomer concentrations within each sectional layer are reported. Segments are drawn to guide the eyes.

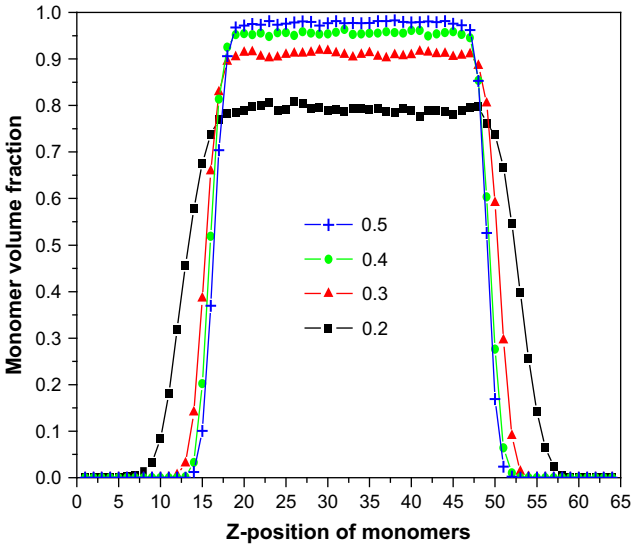

Fig. 5. Monomer distributions along the direction normal to the flat interfaces, i.e. along the *Z*-axis, under variable B/E_C values as denoted with $E_P/E_C = 1$ and $T = 4.5\ E_C/k$. Volume fractions of monomers in each *Z* layer are reported. Segments are drawn to guide the eyes.

monomer concentrations in the segregated polymer phases. Because monomers are homogeneously distributed in bulk phases, these concentrations are roughly equal to polymer volume fractions, which are quantitatively consistent with the predictions shown in Fig. 2.

According to the classical nucleation theory, crystal nucleation is initiated by thermal fluctuations in the homogeneous phase. Only when the size of crystallites exceeds a threshold, can these crystallites survive as crystal nuclei. However, as soon as the critical nuclei have been initiated, irreversible crystal growth prevents us from observing ensemble properties of these crystal nuclei. Since the largest crystallites hold the highest probability to survive as crystal nuclei upon thermal fluctuations, they can represent crystal nuclei in the ensemble statistics. We therefore chose a high temperature, i.e. $4.5\ E_C/k$, at which the spontaneous crystallization will not happen in the time window of our observations, and then we made ensemble statistics on the properties of the largest crystallites.

Since in our simulations the parallel packing of the bonds represented crystalline order, the largest crystallite was defined by the largest amount of crystalline bonds in the crystallite where each crystalline bond contains more than five parallel neighbors. The positional distributions of the largest crystallites along the *Z*-axis are summarized in Fig. 6. One can see that when $B/E_C = 0.2$ and 0.3, the distributions show high flat plateaus in the concentrated polymer phases; but when they become 0.4 and 0.5, double peaks occur. The double peak implies that crystal nucleation gets enhanced near the interfaces, in agreement with the predictions from Fig. 2. This interface-enhanced crystal nucleation confirms the idea proposed by Schaaf et al. on their experimental observations of polyethylene solutions [14]. The similar situation exists in our previous simulations of immiscible polymer blends [13].

The heights of plateaus in Fig. 6 are associated with the thickness of the concentrated phases since the probabilities are normalized over their distributions. Therefore, they reflect only a relative strength of crystal nucleation within the distribution. For this reason, the heights of plateaus cannot be directly compared with each other for strength of crystal nucleation.

The enhancement of crystal nucleation in the concentrated polymer phases can furthermore be observed from the shifting-up

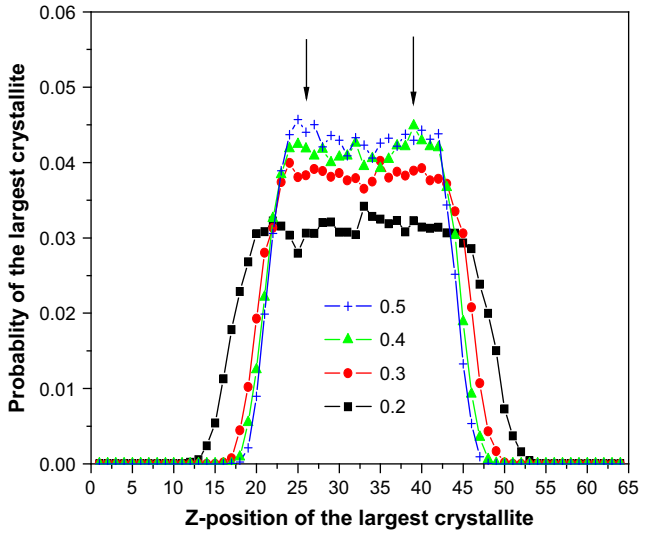

Fig. 6. Positional distributions of the largest crystallites calculated from about 3×10^4 events, while each event is collected with an interval of 200 MC cycles in the evolving systems same as in Fig. 5. Two arrows are indicating the double peak. The segments are drawn to guide the eyes.

of the size distributions of the largest crystallites, as demonstrated in Fig. 7. Note that with the increase of B/E_C values, the shifting-up of size distributions are rather gradual, which are quite different from the corresponding observations on immiscible polymer blends where the shifting-up appears quite a sudden [13]. This difference implies that the enhancement revealed in Fig. 7 could be attributed to the bulk phase rather than the interfaces. Since polymer concentrations in the segregated phases increase gradually with the increase of B/E_C values as demonstrated in Fig. 2, the size distributions of the largest crystallites shift up also gradually. In immiscible polymer blends, in contrast, polymers are strongly segregated, and the enhanced crystal nucleation can be mainly attributed to the diffuse interfaces that exhibit higher melting points but smaller thickness with the increase of B/E_C values. Therefore, in the case of blends, the shifting-up of size distributions of the largest crystallites appears quite a sudden [13].

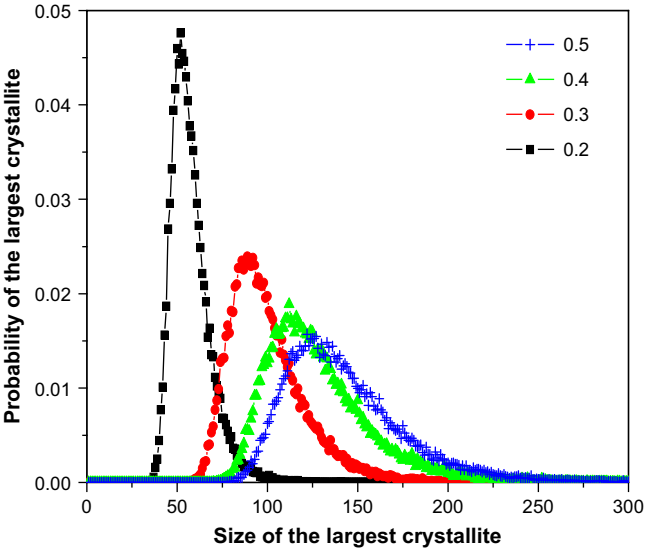

Fig. 7. Size distributions of the largest crystallites calculated under the conditions same as in Fig. 5. The segments are drawn to guide the eyes.

We also calculated the distributions of orientational–order parameters of the largest crystallites along the Z-axis, as demonstrated in Fig. 8. The orientational-order parameter was defined as

$$P = \frac{3\langle \cos^2\theta \rangle - 1}{2}, \tag{7}$$

where the angle θ was the chain axes of the largest crystallites referred to the direction normal to the flat interfaces, and $\langle \cdots \rangle$ meant an ensemble average in each Z layer. According to this definition, when the crystallites are all parallel with interfaces, $P = -0.5$; when they are all perpendicular to interfaces, $P = 1$; and when they are randomly oriented, $P = 0$. Fig. 8 shows that the orientations of the largest crystallites are quite random in the concentrated polymer phase, and near the interfaces a weak preference of perpendicular orientations can be observed. Such a weak preference appears quite general in all the cases, and may be related with the fact that near the interfaces one side of lateral growth of parallel-oriented crystals will be intercepted by the interfaces and these crystals contribute less in the averaged crystal orientations. Therefore, when solvent becomes poor enough, the enhancement of crystal nucleation at the interfaces makes dominantly random orientations of crystals. Similar with immiscible polymer blends, this behavior implies its enthalpic rather than entropic origin [13].

It is worth to note that the entropy-enhanced crystal nucleation at interfaces will exhibit a preference of parallel crystal orientations due to parallel deformation of polymer coils in contact with the repulsive flat wall. Here, we did not observe this preference of crystal orientations, probably because the distances between two parallel interfaces were still much larger than polymer coil sizes [22], and the interfaces can be diffuse in some extents.

In the experiments of dilute solutions of polyethylene, prior spinodal decomposition will generate small spherical domains for the minority of polymers, which gives rise to a spatial confinement for the subsequent polymer crystallization. Such an isolation of the crystallization chambers in small droplets benefits the kinetic study of primary crystal nucleation [23]. Hay and Keller in 1965 [24], and Garber and Geil in 1966 [25], reported the globular particles of crystal aggregates precipitated from poor solvent. Schaaf et al. separated such spherical particles into two parts, i.e. smooth-surface

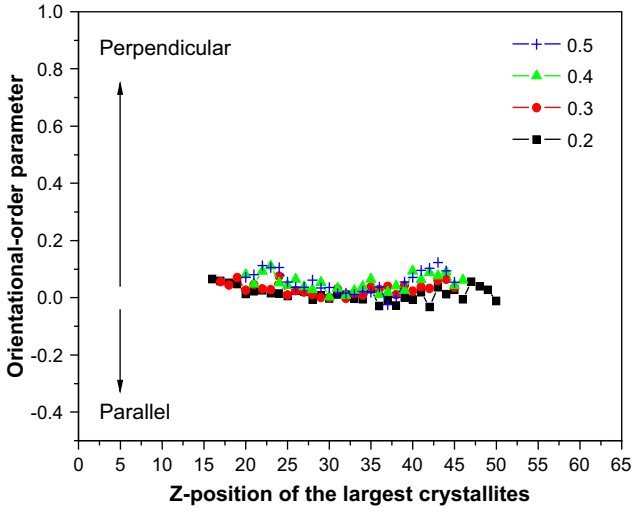

Fig. 8. Distributions of the orientational-order parameters of the largest crystallites along the Z-axis, calculated under the conditions same as in Fig. 5. To avoid the disturbance of bad statistics, the data points are cut off at the number of events less than 100. The reported data are averaged over each Z layer. The segments are drawn to guide the eyes.

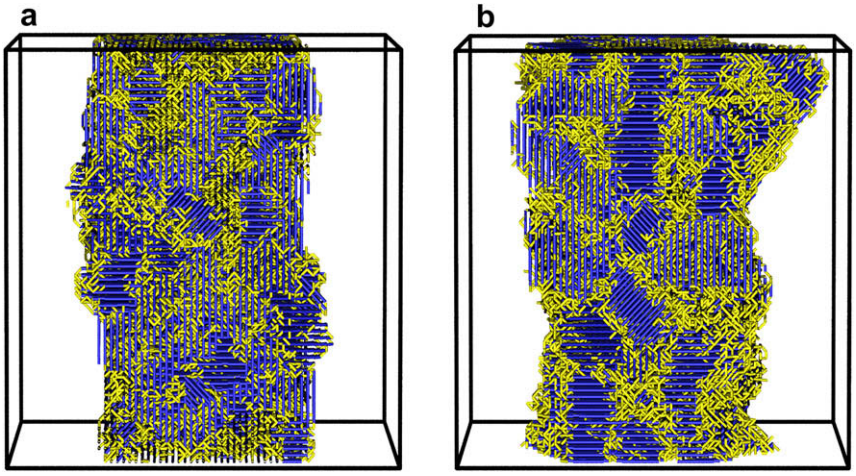

Fig. 9. Snapshots of the segregated polymers after saturate isothermal crystallization at (a) $T = 2.5\ E_C/k$ for 10^5 MC cycles and (b) $T = 3.5\ E_C/k$ for 1.3×10^5 MC cycles with $E_P/E_C = 1$ and $B/E_C = 0.5$. The crystalline bonds that contain more than five parallel neighbors are drawn with tiny cylinders in dark blue, while the other amorphous bonds are drawn with tiny cylinders in bright yellow. (For interpretation of the references to colour in this figure legend, the reader is referred to the web version of this article.)

globules due to homogeneous crystal nucleation and rough-surface globules due to heterogeneous crystal nucleation [14]. They attributed the smoothness of globular crystal aggregates to crystal nucleation initiated at the interfaces, because they suggested that the crystalline stems at the globule surface were oriented in radial directions relative to the center of the globules, and these stems may share the same single lamellar crystal developing along the interface. However, such a strong perpendicular preference of crystal orientations has not been approved by our present simulation results shown in Fig. 8.

In our view, the smoothness at the surface of crystal aggregates may be attributed to the random orientations of vast small crystallites generated at the interfaces under low temperatures. To evidence this argument, we make visual inspections on the surface morphology of segregated polymers prepared by isothermal crystallization at a low temperature in comparison to the case at a relatively high temperature. The snapshots obtained after the saturated crystallization are shown in Fig. 9. One can see that, indeed at low temperatures (see Fig. 9a), vast small crystallites are generated, which make the surface quite smooth on a large scale. In contrast, at high temperatures (see Fig. 9b), less amount of crystallites are generated, and one of them even sticks out of the interface at the up-right corner of the figure, which makes the surface rough. The extreme situation for the more rough surfaces is the heterogeneous nucleation initiated by impurities inside spherical domains at even higher temperatures, which initiates lamellar crystal growth much earlier from the center area and coexists with the homogenous nucleation as proposed by Schaaf et al. [14].

The special bowl-shaped crystal aggregates grown from poor solvent under low temperatures have been found long ago by Khoury and Barnes in their observations of polymer single crystals [26]. Schaaf et al. proposed that the bowl-shaped crystal aggregates should be related with prior liquid-liquid demixing in polymer solutions at low temperatures [14]. This proposition can be supported by the present interface-enhanced polymer crystallization. At the diffuse interfaces, thermodynamic driving forces favor both crystal nucleation and crystal growth. The vast small crystallites are thus generated at low temperatures along the curvature of spherical surfaces of the segregated polymer domains, till most of amorphous polymers have been exhausted in the concentrated phase to form the bowl-shaped crystal aggregates. Indeed, shrunken hollow globules formed in poor solvent have been observed by Schaaf et al. which led to their proposition of interface-induced crystal nucleation [14].

The similar situation is the semi-hexagons or strings of semi-hexagons of poly(l-benzyl-L-glutamate) grown in poor solvent as reported by Price et al. [27]. Schaaf et al. have considered such a case as crystal nucleation initiated near interfaces, which again made a restriction to the global shapes of crystalline domains [14].

5. Conclusions

Theoretical phase diagrams of polymer solutions show that at the chosen crystallization temperatures near the concentrated end, the melting points of segregated polymers increase with the poor quality of solvent. In addition, only when solvent becomes poor enough, can the melting points at diffuse interfaces be higher than those in the bulk phase. Sharing the same crystallization temperatures, a higher melting point implies a larger thermodynamic driving force for crystal nucleation. So crystal nucleation will be enhanced with higher melting points.

The dynamic Monte Carlo simulations verified the enhanced polymer crystal nucleation with the increase of the poor solvent quality in the concentrated phase after the equilibrium of phase separation has been well established in solutions. Furthermore, beyond a critically quality of poor solvent, the diffuse interfaces make an enhancement of crystal nucleation. The interface-enhanced crystal nucleation is similar with our previous observations on the immiscible polymer blends. Such an enhancement evidences the previous interpretation [14] to the experimental observations on the bowl-shaped abnormal crystal morphology of polyethylene grown in poor solvent.

The enhancement of crystal nucleation by poorer solvent, and the critical quality of poor solvent to observe the interface-enhanced crystal nucleation, both are the properties of solution-segregated polymers different from blend-segregated polymers. This uniqueness can be attributed to the strong mixing entropy in the mixing free energy of polymer solutions, which causes a local melting-point depression upon dilution from the concentrated end.

In a broader sense, the interplay of phase transitions exists not only in the intermolecular mixtures but also in the intramolecular multi-component systems such as block copolymers, gradient copolymers, and statistical copolymers. Further investigation of such interplay in these polymers and their mixtures will facilitate our better understanding of the complexity and the richness of polymer morphologies upon self-assembly of multi-component polymeric systems.

Acknowledgements

WH thanks the helpful discussions with Prof. Bernard Lots at Institute Charles Sadron, Strasbourg, France. We appreciate the financial supports from National Natural Science Foundation of China (NSFC Grant Nos. 20474027, 20674036, and 20825415) and State Key Laboratory for Modification of Chemical Fibers and Polymer Materials at Donghua University of China.

References

[1] Richards RB. Trans Faraday Soc 1946;42:10–28.
[2] Flory PJ. Principles of polymer chemistry. Ithaca, NY: Cornell University Press; 1953.
[3] Cheng SZD. Phase transitions in polymers. Amsterdam: Elsevier; 2008.
[4] Keller A. Faraday Discuss 1995;101:1–49.
[5] Graham PD, McHugh AJ. Macromolecules 1998;31:2565–8.
[6] Hu WB, Frenkel D. Macromolecules 2004;37:4336–8.
[7] Zha LY, Hu WB. J Phys Chem B 2007;111:11373–8.
[8] Hu WB, Frenkel D. J Phys Chem B 2006;110:3734–7.
[9] Wang H, Shimizu K, Kim H, Hobbie EK, Wang ZG, Han CC. J Chem Phys 2002;116:7311–5.
[10] Hu WB, Mathot VBF. J Chem Phys 2003;119:10953–7.
[11] Ma Y, Hu WB, Wang H. Phys Rev E 2007;76:031801.
[12] (a) Zhang XH, Wang ZG, Muthukumar M, Han CC. Macromol Rapid Commun 2005;26:1285–8;
(b) Zhang XH, Wang ZG, Dong X, Wang DJ, Han CC. J Chem Phys 2006; 125:024907;
(c) Zhang XH, Wang ZG, Zhang RY, Han CC. Macromolecules 2006;39: 9285–90;
(d) Niu YH, Wang ZG, Orta CA, Xu DH, Wang H, Shimizu K, et al. Polymer 2007;48:6668–80.
[13] Ma Y, Zha LY, Hu WB, Reiter G, Han CC. Phys Rev E 2008;77:061801.
[14] Schaaf P, Lotz B, Wittmann JC. Polymer 1987;28:193–200.
[15] (a) Meyer KH. Z Phys Chem, Leipzig 1939;44:383–91;
(b) Flory PJ. J Chem Phys 1942;10:51–61;
(c) Huggins ML. Ann N Y Acad Sci 1942;43:1–32.
[16] (a) Scott RL. J Chem Phys 1949;17:279–84;
(b) Tompa H. Trans Faraday Soc 1949;45:1142–52.
[17] Flory PJ. Proc R Soc Lond, Ser A 1956;234:60–73.
[18] Leibler L. Macromolecules 1980;13:1602–17.
[19] Flory PJ, Rehner Jr J. J Chem Phys 1943;11:521–6.
[20] Hu WB. J Chem Phys 2000;113:3901–8.
[21] (a) Hu WB, Mathot VBF, Frenkel D. J Chem Phys 2003;118:10343–8;
(b) Hu WB, Frenkel D. Adv Polymer Sci 2005;191:1–35.
[22] Ma Y, Hu WB, Reiter G. Macromolecules 2006;39:5159–64.
[23] (a) Cormia RL, Price FP, Turnbull D. J Chem Phys 1962;37:1333–40;
(b) Ross GS, Frolen LJ. J Res Natl Bur Stand A 1975;79:701–11.
[24] Hay IL, Keller A. Kolloid Z Z Polym 1965;204:43–74.
[25] Garber CA, Geil PH. J Appl Phys 1966;37:4034–40.
[26] (a) Khoury F, Barnes JD. J Res Natl Bur Stand A 1972;76:225–52;
(b) Khoury F, Barnes JD. J Res Natl Bur Stand A 1974;78:95–127;
(c) Barnes JD, Khoury F. J Res Natl Bur Stand A 1974;78:363–73.
[27] (a) Price C, Harris PA, Holton TJ, Stubbersfield RB. Polymer 1975;16:69–71;
(b) Price C, Holton TJ, Stubbersfield RB. Polymer 1979;20:1059–61.